View metadata, citation and similar papers at core.ac.uk

brought to you by CORE

provided by Tsukuba Repository

# Theoretical Study on Quantum Dynamics of Coherent Phonon Generation in the Early-Time Region

| | |
|---|---|
| 著者 | Watanabe Yohei |
| 内容記述 | この博士論文は内容の要約のみの公開（または一部非公開）になっています |
| year | 2018 |
| その他のタイトル | 初期時間領域におけるコヒーレントフォノン生成量子ダイナミックスの理論研究 |
| 学位授与大学 | 筑波大学 (University of Tsukuba) |
| 学位授与年度 | 2017 |
| 報告番号 | 12102甲第8485号 |
| URL | http://hdl.handle.net/2241/00152366 |

Graduate School of Pure and Applied Sciences

# Theoretical Study on Quantum Dynamics of Coherent Phonon Generation in the Early-Time Region

（初期時間領域におけるコヒーレントフォノン生成量子ダイナミックスの理論研究）

Yohei Watanabe

Doctoral Program in Materials Science
Student ID Number 201530117
Doctor of Philosophy in Engineering
Advised by Ken-ichi Hino

## 1 Introduction

The development of the technology for ultrashort pulse laser with high intensity has enabled us to explore a new research area of ultrafast and non-equilibrium phenomena governed by heavily photoexcited carriers. Coherent phonon (CP) generation [1] is one of the representative ultrafast phenomena unveiled by the irradiation of the ultrashort pulse laser, and this has been investigated in a variety of materials such as semiconductors, semimetals/metals, superconductors, and other materials [2, 3, 4, 5]. Here, a longitudinal optical (LO) phonon is driven by the pulse whose temporal width is much shorter than a period of the LO phonon, namely of an order of 10 fs. Thus far, the CP generation mechanism has been discussed by means of classical models based on a damped forced-oscillation, and a great number of experimental results have been examined from the viewpoint of a phase shift built in an asymptotic harmonic vibration, termed as an initial phase.

Two well-known classical models have been employed for the discussion on the CP generation thus far. One is the impulsive stimulated Raman scattering model [6], and in this model, it is considered that a delta function-shaped force attributed to Raman polarizability drives the oscillator, resulting in the sine form. The other is the displacive excitation of CP model [7], where the external force is associated with the photoexcited carriers of a step function-like shape, and the oscillation becomes of the cosine form. These classical models have succeeded in revealing overall character of the CP generation dynamics, and have been followed by associated theoretical studies [8, 9].

However, it is a matter of course that such approaches encounter difficulties in revealing unexplored quantum effects in addition to demonstrating the details of the CP dynamics of concern embedded in the initial phases. Quantum effects arise in the early stage of the CP generation where heavily photoexcited carriers interact with an LO phonon; hereafter, we term this time region the early time region (ETR). Incidentally in fact, additional complicated signals due to nonlinear optical interference, termed as coherent artifact [10], manifest themselves in the ETR, which result in masking inherent dynamics in CP.

As regards the quantum effect accompanied by the CP generation, Fano resonance (FR) [11] has been observed transiently in the ETR for lightly $n$-doped Si [2]. This FR is considered to be caused by interference between a discrete state of the LO phonon and continuum states of the excited carriers. This is discerned just in a moment before the carrier relaxation time. Further, it is speculated that the manifestation of the FR is the vestige of the birth of a polaronic quasiparticle (PQ) due to the strong carrier-LO phonon interaction [12]. Here, we stress that the concerned transient FR is distinct from the FR observed in incoherent Raman scattering for heavily doped Si [13].

The aim of the present dissertation is as follows. First, we construct a fully quantum mechanical model for the CP generation dynamics applicable for both nonpolar and polar semiconductors on an equal footing [14]. In this model, we introduce PQ operators on the basis of the supposition of the transient formation of the PQ in the experiments [2, 12], and these operators are composed of an LO phonon operator and a set of pairs of electron operators. Next, on the basis of this PQ model, we inspect the origin of the transient FR and other unexplored quantum effects [14, 15]. Further, we investigate features of the CP generation such as the initial phases and the asymptotic amplitudes under various pulse laser conditions [15]. For these purposes, we examine a retarded longitudinal susceptibility related to transient induced photoemission spectra and a CP displacement function.

This summary is organized as follows. In Sec. 2, we provide the brief explanation of the theoretical framework. In Secs. 3 and 4, we present the results and discussion, and the conclusion, respectively. Atomic units (a.u.) are used throughout unless otherwise stated.

# 2 Theory

## 2.1 Equations of motion

We take into consideration the total Hamiltonian $\hat{H} = \hat{H}_e + \hat{H}'(t) + \hat{H}_p + \hat{H}_{e-p}$. A two-band electron Hamiltonian is given by $\hat{H}_e = \sum_{b\boldsymbol{k}} \varepsilon_{b\boldsymbol{k}} a^\dagger_{b\boldsymbol{k}} a_{b\boldsymbol{k}} + (1/2) \sum_{\boldsymbol{q}\neq 0} V^{(C)}_{\boldsymbol{q}} \sum_{bb'\boldsymbol{k}\boldsymbol{k}'} a^\dagger_{b\boldsymbol{k}+\boldsymbol{q}} a^\dagger_{b'\boldsymbol{k}'-\boldsymbol{q}} a_{b'\boldsymbol{k}'} a_{b\boldsymbol{k}}$. Conduction and valence bands are labeled as $b = c$ and $b = v$, respectively. $a^\dagger_{b\boldsymbol{k}}$ and $a_{b\boldsymbol{k}}$ represent creation and annihilation operators of an electron, respectively. Here, an energy dispersion in band $b$ and a Coulomb potential are provided by $\varepsilon_{b\boldsymbol{k}}$ and $V^{(C)}_{\boldsymbol{q}}$, respectively with the Bloch momentum $\boldsymbol{k}$ and $\boldsymbol{q}$. The electron-light interaction at time $t$ is given by $\hat{H}'(t) = -\sum_{\boldsymbol{k}} \left[ \Omega_{cv}(t)\, a^\dagger_{c\boldsymbol{k}} a_{v\boldsymbol{k}} + \Omega_{vc}(t)\, a^\dagger_{v\boldsymbol{k}} a_{c\boldsymbol{k}} \right]$, and $\Omega_{b\bar{b}}(t)$ with $\bar{b} \neq b$ is expressed as

$$\Omega_{b\bar{b}}(t) = \Omega_{0b\bar{b}} f(t) \cos\omega_0 t, \tag{1}$$

where the Rabi frequency $\Omega_{0b\bar{b}}$ is provided by the product of a peak amplitude of an irradiated electric field and the electric dipole moment between $\Gamma$-points of $c$- and $v$-bands. Further, $\omega_0$ and $f(t)$ are laser frequency and a pulse-envelope function, respectively. An LO phonon Hamiltonian and the electron-phonon interaction are given by $\hat{H}_p = \sum_{\boldsymbol{q}} \omega_{\boldsymbol{q}} c^\dagger_{\boldsymbol{q}} c_{\boldsymbol{q}}$ and $\hat{H}_{e-p} = \sum_{b\boldsymbol{q}\boldsymbol{k}} \left( g_{b\boldsymbol{q}} c_{\boldsymbol{q}} a^\dagger_{b\boldsymbol{k}+\boldsymbol{q}} a_{b\boldsymbol{k}} + g^*_{b\boldsymbol{q}} c^\dagger_{\boldsymbol{q}} a^\dagger_{b\boldsymbol{k}} a_{b\boldsymbol{k}+\boldsymbol{q}} \right)$, respectively. $c^\dagger_{\boldsymbol{q}}$ and $c_{\boldsymbol{q}}$ represent creation and annihilation operators of LO phonon, respectively, with energy dispersion $\omega_{\boldsymbol{q}}$. It is considered that the LO phonon mode is coupled with $b$-band electron through the interaction represented by a coupling constant $g_{b\boldsymbol{q}}$.

The non-equilibrium dynamics driven by the pump laser irradiation of concern is described by time-evolution of the phonon operator and a composite operator representing an induced carrier density, defined as $A^\dagger_{\boldsymbol{q}}(\boldsymbol{k}bb') = a^\dagger_{b\boldsymbol{k}+\boldsymbol{q}} a_{b'\boldsymbol{k}}$. It is remarked that we are concerned exclusively with the case of $\boldsymbol{q}$ being quite small, but finite: $\boldsymbol{q} \neq 0$. In terms of the Heisenberg equation, the equation of motion of $A^\dagger_{\boldsymbol{q}}(\boldsymbol{k}bb')$ is expressed as

$$-i \left( \frac{d}{dt} + \frac{1}{T_{\boldsymbol{q}\boldsymbol{k}bb'}} \right) A^\dagger_{\boldsymbol{q}}(\boldsymbol{k}bb') = [\hat{H}_e + \hat{H}'(t), A^\dagger_{\boldsymbol{q}}(\boldsymbol{k}bb')] + [\hat{H}_{e-p}, A^\dagger_{\boldsymbol{q}}(\boldsymbol{k}bb')], \tag{2}$$

where a time constant $T_{\boldsymbol{q}\boldsymbol{k}bb'}$ describes a phenomenological relaxation of $A^\dagger_{\boldsymbol{q}}(\boldsymbol{k}bb')$. We obtain the expression of the first commutator in the right-hand side of Eq. (2) as $[\hat{H}_e + \hat{H}'(t), A^\dagger_{\boldsymbol{q}}(\boldsymbol{k}bb')] \approx \sum_{\tilde{\boldsymbol{k}}\tilde{b}\tilde{b}'} A^\dagger_{\boldsymbol{q}}(\tilde{\boldsymbol{k}}\tilde{b}\tilde{b}') Z_{\boldsymbol{q}}(\tilde{\boldsymbol{k}}\tilde{b}\tilde{b}', \boldsymbol{k}bb')$, where $Z_{\boldsymbol{q}}$ represents a $c$-number non-Hermitian matrix, though an explicit form is not shown here. It is noted that we evaluate Eq. (2) by employing a factorization approximation, and split four operator terms such as $a^\dagger_{\tilde{b},\tilde{\boldsymbol{k}}+\tilde{\boldsymbol{q}}} a_{\tilde{b}'\tilde{\boldsymbol{k}}} a^\dagger_{b,\boldsymbol{k}+\boldsymbol{q}} a_{b'\boldsymbol{k}}$ into a product of

$A^\dagger_{\boldsymbol{q}}(\tilde{\boldsymbol{k}}\tilde{b}\tilde{b}')$ and a single-particle density matrix $\rho_{bb'\boldsymbol{k}} \equiv \langle a^\dagger_{b\boldsymbol{k}} a_{b'\boldsymbol{k}} \rangle$, where $\langle \hat{O} \rangle$ represents an expectation value of an operator $\hat{O}$ concerning the ground state. Moreover, we employ the rotating wave approximation, and thus high-frequency contributions are removed; $A^\dagger_{\boldsymbol{q}}(\boldsymbol{k}bb')$, $\rho_{bb'\boldsymbol{k}}$, and $Z_{\boldsymbol{q}}(\tilde{\boldsymbol{k}}\tilde{b}\tilde{b}', \boldsymbol{k}bb')$ are replaced by $e^{i\bar{\omega}_{bb'}t}\bar{A}^\dagger_{\boldsymbol{q}}(\boldsymbol{k}bb')$, $e^{i\bar{\omega}_{bb'}t}\bar{\rho}_{bb'\boldsymbol{k}}$, and $\bar{Z}_{\boldsymbol{q}}(\tilde{\boldsymbol{k}}\tilde{b}\tilde{b}', \boldsymbol{k}bb')$, respectively, where $\bar{\omega}_{cv} = \omega_0$, $\bar{\omega}_{vc} = -\omega_0$, and $\bar{\omega}_{bb} = 0$. Therefore, Eq. (2) becomes of the form

$$
\begin{aligned}
-i\left(\frac{d}{dt} + \frac{1}{T_{\boldsymbol{q}\boldsymbol{k}bb'}}\right)\bar{A}^\dagger_{\boldsymbol{q}}(\boldsymbol{k}bb') &= [\hat{H}_e + \hat{H}'(t), \bar{A}^\dagger_{\boldsymbol{q}}(\boldsymbol{k}bb')] - \bar{A}^\dagger_{\boldsymbol{q}}(\boldsymbol{k}bb')\bar{\omega}_{bb'} + [\hat{H}_{e-p}, \bar{A}^\dagger_{\boldsymbol{q}}(\boldsymbol{k}bb')] \\
&\approx \sum_{\tilde{\boldsymbol{k}}\tilde{b}\tilde{b}'} \bar{A}^\dagger_{\boldsymbol{q}}(\tilde{\boldsymbol{k}}\tilde{b}\tilde{b}')\bar{Z}_{\boldsymbol{q}}(\tilde{\boldsymbol{k}}\tilde{b}\tilde{b}', \boldsymbol{k}bb') + [\hat{H}_{e-p}, \bar{A}^\dagger_{\boldsymbol{q}}(\boldsymbol{k}bb')]. \qquad (3)
\end{aligned}
$$

As regards the equation of motion of $c^\dagger_{\boldsymbol{q}}$, it is straightforward derived as $-i\frac{dc^\dagger_{\boldsymbol{q}}}{dt} = \omega_{\boldsymbol{q}} c^\dagger_{\boldsymbol{q}} + \sum_{b\boldsymbol{k}} g_{b\boldsymbol{q}} \bar{A}^\dagger_{\boldsymbol{q}}(\boldsymbol{k}bb)$.

### 2.2 Physical quantities

On the basis of the linear response theory, an induced charge density $n^{(ind)}_{\boldsymbol{q}}(t)$ caused by a weak external field $f_{\boldsymbol{q}}(t)$ is given by $n^{(ind)}_{\boldsymbol{q}}(t) = -\int_{-\infty}^{t} dt'\, \chi^{(t)}_{\boldsymbol{q}}(t,t') f_{\boldsymbol{q}}(t')/4\pi V$ [16], where $V$ is a volume of a crystal. $\chi^{(t)}_{\boldsymbol{q}}(t,t')$ is a retarded longitudinal susceptibility in the non-equilibrium and transient system of concern, and it consists of two contributions as [16]

$$
\chi^{(t)}_{\boldsymbol{q}}(t,t') = \chi_{\boldsymbol{q}}(t,t') + \chi'_{\boldsymbol{q}}(t,t'), \qquad (4)
$$

where $\chi_{\boldsymbol{q}}(t,t')$ and $\chi'_{\boldsymbol{q}}(t,t')$ are retarded susceptibilities attributed to an electron-induced interaction and an LO phonon-induced interaction, respectively. The two susceptibilities are proportional to a retarded density-density correlation function of electrons expressed as $D^R_{\boldsymbol{q}}(t,t')$, and a retarded phonon Green function expressed as $D'^R_{\boldsymbol{q}}(t,t')$, respectively. $D^R_{\boldsymbol{q}}(t,t')$ is provided by $D^R_{\boldsymbol{q}}(t,t') = -i\langle[\hat{n}_{\boldsymbol{q}}(t), \hat{n}_{-\boldsymbol{q}}(t')]\rangle\theta(t-t')$, with a density operator $\hat{n}_{\boldsymbol{q}}(t) = \sum_{b\boldsymbol{k}} a^\dagger_{b\boldsymbol{k}+\boldsymbol{q}} a_{b\boldsymbol{k}}/V$. On the other hand, $D'^R_{\boldsymbol{q}}(t,t')$ is provided by $D'^R_{\boldsymbol{q}}(t,t') = -i\langle[c_{\boldsymbol{q}}(t) + c^\dagger_{-\boldsymbol{q}}(t), c_{-\boldsymbol{q}}(t') + c^\dagger_{\boldsymbol{q}}(t')]\rangle\theta(t-t')$.

We investigate two physical quantities associated with the retarded susceptibilities; a transient induced photoemission spectrum and a CP displacement function. The dielectric function $\epsilon_{\boldsymbol{q}}(t_p+\tau, t_p)$ is straightforward derived from $\chi^{(t)}_{\boldsymbol{q}}(t_p+\tau, t_p)$, and $t_p$ is the time where $f_{\boldsymbol{q}}(t')$ probes dynamics of concern. Here, it is remarked that $\epsilon_{\boldsymbol{q}}(t_p+\tau, t_p)$ and $\chi^{(t)}_{\boldsymbol{q}}(t_p+\tau, t_p)$ are dependent on $t_p$ in addition to the relative time $\tau = t - t'$, which is distinct from equilibrium systems. Thus, the Fourier transform of $\epsilon_{\boldsymbol{q}}(t_p+\tau, t_p)$ as $\tilde{\epsilon}_{\boldsymbol{q}}(t_p;\omega) = \int_0^\infty d\tau e^{-i\omega\tau}\epsilon_{\boldsymbol{q}}(t_p+\tau, t_p)$ leads to the transient induced photoemission spectra defined by $\bar{I}_{\boldsymbol{q}}(t_p;\omega) = -\mathrm{Im}\tilde{\epsilon}_{\boldsymbol{q}}(t_p;\omega)$. On the other hand, the CP displacement function $Q_{\boldsymbol{q}}(\tau)$ is provided by $Q_{\boldsymbol{q}}(\tau) = D^R_{\boldsymbol{q}}(\tau+t', t') - D^{R(0)}_{\boldsymbol{q}}(\tau+t', t')$ except for a trivial proportional constant. Here $t' = 0$ is concerned, and the retarded free phonon Green function $D^{R(0)}_{\boldsymbol{q}}(t,t') = -2\sin[\omega_{\boldsymbol{q}}(t-t')]\theta(t-t')$ is subtracted. $Q_{\boldsymbol{q}}(\tau)$ is expressed as $Q_{\boldsymbol{q}}(\tau) = C_{\boldsymbol{q}}(\tau)\cos[\omega_{\boldsymbol{q}}\tau + \Theta_{\boldsymbol{q}}(\tau)]$, where $C_{\boldsymbol{q}}(\tau)$ and $\Theta_{\boldsymbol{q}}(\tau)$ are a transitory amplitude and a renormalized phase modulus $\pi$ at $\tau$. After the ETR, $C_{\boldsymbol{q}}(\tau)$ and $\Theta_{\boldsymbol{q}}(\tau)$ become an asymptotic amplitude $C^0_{\boldsymbol{q}}$ and an initial phase $\theta_{\boldsymbol{q}}$, respectively.

### 2.3 Polaronic quasiparticle operators

We suppose the PQ suggested in the experiments [2, 12], and define the PQ operator composed of $\bar{A}^\dagger_{\boldsymbol{q}}(\boldsymbol{k}bb')$ and $c^\dagger_{\boldsymbol{q}}$. Brief explanations of the PQ are shown in the following. First of all, we solve an eigenvalue problem of the non-Hermitian matrix $\bar{Z}_{\boldsymbol{q}}$ in Eq. (3) with $t$ fixed as an adiabatic parameter, represented by $U^{L\dagger}_{\boldsymbol{q}}\bar{Z}_{\boldsymbol{q}} = \mathcal{E}_{\boldsymbol{q}}U^{L\dagger}_{\boldsymbol{q}}$ and $\bar{Z}_{\boldsymbol{q}}U^R_{\boldsymbol{q}} = U^R_{\boldsymbol{q}}\mathcal{E}_{\boldsymbol{q}}$. $U^L_{\boldsymbol{q}}$ and $U^R_{\boldsymbol{q}}$

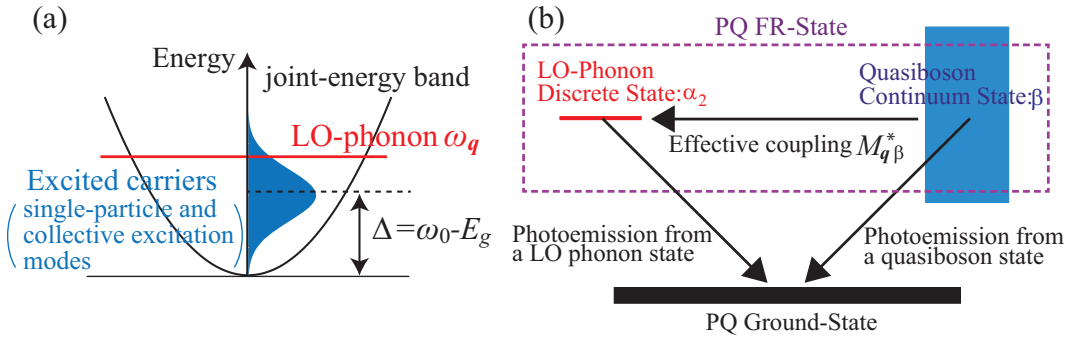


Figure 1: Schematic diagrams of (a) the energy distribution due to the photoexcited carriers, and (b) the transient FR dynamics based on the PQ picture. (From Refs. [14] and [15] with partial modification.)

are biorthogonal left and right eigenvectors, respectively with an adiabatic eigenvalue diagonal matrix $\mathcal{E}_{\boldsymbol{q}}$. We employ matrix notations, that is, $\bar{Z}_{\boldsymbol{q}} = \left\{\bar{Z}_{\boldsymbol{q}}(\tilde{\boldsymbol{k}}\tilde{b}\tilde{b}', \boldsymbol{k}bb')\right\}$, $\mathcal{E}_{\boldsymbol{q}} = \{\mathcal{E}_{\boldsymbol{q}\alpha}\}$, and $U^{L/R}_{\boldsymbol{q}} = \left\{U^{L/R}_{\boldsymbol{q}\alpha}(\boldsymbol{k}bb')\right\}$, where $\mathcal{E}_{\boldsymbol{q}\alpha}$ and $U^{L/R}_{\boldsymbol{q}\alpha}(\boldsymbol{k}bb')$ represent the eigenvalue and eigenvector of the $\alpha$th state, respectively. Here, the set of eigenstates $\{\alpha\}$ consists of a single discrete state of the plasmonlike mode signified as $\alpha_1$, and a continuum state of single-particle excitation modes signified as $\{\beta\}$, namely $\{\alpha, \alpha'\} = (\alpha_1, \{\beta\})$. Here, we define the creation operator of an quasiboson of the $\alpha$th state as $B^\dagger_{\boldsymbol{q}\alpha} = \sum_{\boldsymbol{k}bb'} \bar{A}^\dagger_{\boldsymbol{q}}(\boldsymbol{k}bb')U^R_{\boldsymbol{q}\alpha}(\boldsymbol{k}bb')$, and furthermore, an effective quasiboson-phonon coupling constants are given by $M_{\boldsymbol{q}\alpha} = \sum_{\boldsymbol{k}b} g_{b\boldsymbol{q}} U^{L\dagger}_{\boldsymbol{q}\alpha}(\boldsymbol{k}bb)$ and $M'^*_{\boldsymbol{q}\alpha} = \sum_{\alpha'} M^*_{\boldsymbol{q}\alpha'}\langle[B_{\boldsymbol{q}\alpha'}, B^\dagger_{\boldsymbol{q}\alpha}]\rangle = \sum_{\boldsymbol{k}bb'}\left(g^*_{b\boldsymbol{q}}\bar{\rho}_{bb'\boldsymbol{k}} - g^*_{b'\boldsymbol{q}}\bar{\rho}_{bb'\boldsymbol{k}+\boldsymbol{q}}\right)U^R_{\boldsymbol{q}\alpha}(\boldsymbol{k}bb')$.

Thus, the equations of motion of $B^\dagger_{\boldsymbol{q}\alpha}$ and $c^\dagger_{\boldsymbol{q}}$ are integrated into a single equation in a matrix form of $-i\frac{d}{dt}[B^\dagger_{\boldsymbol{q}}, c^\dagger_{\boldsymbol{q}}] \approx [B^\dagger_{\boldsymbol{q}}, c^\dagger_{\boldsymbol{q}}]h_{\boldsymbol{q}} + [iB^\dagger_{\boldsymbol{q}}\mathcal{W}_{\boldsymbol{q}}, 0]$, where $\mathcal{W}_{\boldsymbol{q}} = \{\mathcal{W}_{\boldsymbol{q}\alpha\alpha'}\}$ and $\mathcal{W}_{\boldsymbol{q}\alpha'\alpha} \equiv \sum_{\boldsymbol{k}bb'}[dU^{L\dagger}_{\boldsymbol{q}\alpha'}(\boldsymbol{k}bb')/dt]U^R_{\boldsymbol{q}\alpha}(\boldsymbol{k}bb') + \sum_{\boldsymbol{k}bb'} U^{L\dagger}_{\boldsymbol{q}\alpha'}(\boldsymbol{k}bb')T^{-1}_{\boldsymbol{q}\boldsymbol{k}bb'}U^R_{\boldsymbol{q}\alpha}(\boldsymbol{k}bb')$. Further, $h_{\boldsymbol{q}} \equiv \{h_{\boldsymbol{q}\gamma\gamma'}\}$ is a non-Hermitian matrix provided by $h_{\boldsymbol{q}} = \begin{bmatrix} \mathcal{E}_{\boldsymbol{q}} & M_{\boldsymbol{q}} \\ M'^\dagger_{\boldsymbol{q}} & \omega_{\boldsymbol{q}} \end{bmatrix}$. Here, $\{\gamma, \gamma'\} = (\{\beta\}, \alpha_1, \alpha_2)$ with $\alpha_2$ representing a LO phonon mode and $\gamma, \gamma' = 1 \sim N+2$, where $N$ is the number of the single-particle excitation modes; $\beta, \beta' = 1 \sim N$.

We are exclusively concerned with the case where the continuum level of $\{\beta\}$ overlaps the two discrete levels of $\alpha_1$ and $\alpha_2$. This case is categorized into the Fano problem, in other words, the multichannel scattering problem with one open channel and two closed channels, except for $h_{\boldsymbol{q}}$ being non-Hermitian. We take into account the following coupled equations of $\sum_{\gamma'} h_{\boldsymbol{q}\gamma\gamma'}V^R_{\boldsymbol{q}\gamma'\beta} = V^R_{\boldsymbol{q}\gamma\beta}\mathcal{E}_{\boldsymbol{q}\beta}$, where $V^R_{\boldsymbol{q}\beta} = \{V^R_{\boldsymbol{q}\gamma\beta}\}$ represents the right vector of the solution for given energy $\mathcal{E}_{\boldsymbol{q}\beta}$. In terms of $V^R_{\boldsymbol{q}\beta}$, we define a set of $N$ operators $F^\dagger_{\boldsymbol{q}\beta}$ as $F^\dagger_{\boldsymbol{q}\beta} = \sum_{\beta'} B^\dagger_{\boldsymbol{q}\beta'}V^R_{\boldsymbol{q}\beta'\beta} + B^\dagger_{\boldsymbol{q}\alpha_1}V^R_{\boldsymbol{q}\alpha_1\beta} + c^\dagger_{\boldsymbol{q}}V^R_{\boldsymbol{q}\alpha_2\beta}$. Further, we introduce the left vector $V^{L\dagger}_{\boldsymbol{q}\beta} = \{V^{L\dagger}_{\boldsymbol{q}\beta\gamma}\}$ associated with $V^R_{\boldsymbol{q}\beta}$ in order to satisfy the inverse relations $B^\dagger_{\boldsymbol{q}\alpha} = \sum_\beta F^\dagger_{\boldsymbol{q}\beta}V^{L\dagger}_{\boldsymbol{q}\beta\alpha}$ and $c^\dagger_{\boldsymbol{q}} = \sum_\beta F^\dagger_{\boldsymbol{q}\beta}V^{L\dagger}_{\boldsymbol{q}\beta\alpha_2}$, where $\sum_\gamma V^{L\dagger}_{\boldsymbol{q}\beta\gamma}V^R_{\boldsymbol{q}\gamma\beta'} = \delta_{\beta\beta'}$ and $\sum_\beta V^R_{\boldsymbol{q}\gamma\beta}V^{L\dagger}_{\boldsymbol{q}\beta\gamma'} = \delta_{\gamma\gamma'}$. Thus, we investigate time-evolution of $F^\dagger_{\boldsymbol{q}\beta}$ in terms of the associated Heisenberg equation. Employing the inverse relations, we obtain expressions of the retarded Green functions in terms of $F^\dagger_{\boldsymbol{q}\beta}$, though not shown here.

Finally, in Fig. 1, we show the diagrams representing the transient FR dynamics concomitant with the CP generation on the basis of the PQ picture. As shown in Fig. 1(a), in the joint-band energy dispersion, the carriers form the energy distribution depending on the Rabi frequency

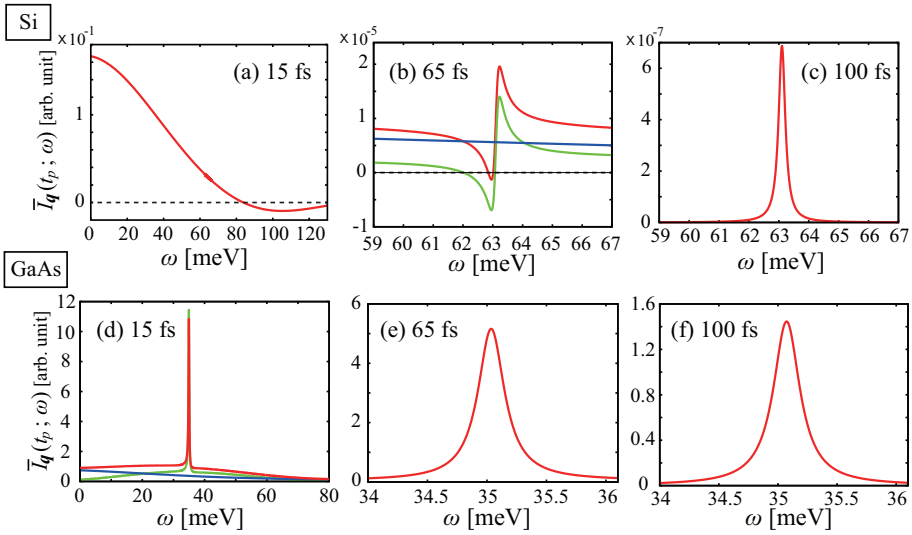


Figure 2: Transient photoemission spectra $\bar{I}_{\boldsymbol{q}}(t_p;\omega)$ as a function of $\omega$ for Si at probe time $t_p$ of (a) 15 fs, (b) 65 fs, and (c) 100 fs, and those for GaAs at $t_p$ of (d) 15 fs, (e) 65 fs, and (f) 100fs. (From Ref. [14] with partial modification.)

$\Omega_{0cv}$ in Eq. (1), the pulse width defined by $\tau_L$, and the detuning defined as

$$\Delta = \omega_0 - E_g, \tag{5}$$

where $E_g$ represents a band gap energy at $\Gamma$ point. Further, the energy distribution partially overlaps with the energy of the LO phonon $\omega_{\boldsymbol{q}}$. As shown in Fig. 1(b), the PQ FR state constituted of the $\alpha_2$ and $\beta$ states is deexcited through an induced photoemission process. The detail of the deexcitation process is discussed in Sec. 3.1. It is noted that the contribution of the $\alpha_1$ state to the transient FR is negligibly small.

# 3 Results and Discussion

## 3.1 Transient Fano resonance

In this section, the numerical calculations are conducted with $\Omega_{0cv} = 16.5$ meV and $\Delta = 82$ meV for undoped Si, and $\Omega_{0cv} = 27.2$ meV and $\Delta = 73$ meV for undoped GaAs. The pulse-envelop function $f(t)$ in Eq. (1) is set to a squared shape with $\tau_L = 15$ fs. It is noted that we assume $\langle [B_{\boldsymbol{q}\alpha}, B^{\dagger}_{\boldsymbol{q}'\alpha'}] \rangle = \delta_{\boldsymbol{q}\boldsymbol{q}'}\delta_{\alpha\alpha'}$ is fulfilled, so that the effective coupling $M'_{\boldsymbol{q}\alpha}$ becomes equal to $M_{\boldsymbol{q}\alpha}$. This assumption is verified by partially neglecting the effects of the interband density matrices $\bar{\rho}_{b\bar{b}\boldsymbol{k}}$. As a result, the matrix $h_{\boldsymbol{q}}$ becomes Hermitian, and $V^L_{\boldsymbol{q}\beta}$ and $V^R_{\boldsymbol{q}\beta}$ become equivalent, which enables one to employ the solutions of the Fano problem as a set of the vectors [17].

The transient induced photoemission spectrum $\bar{I}_{\boldsymbol{q}}(t_p;\omega)$ is a decisive observable to comprehend the occurrence of transient and nonlinear FR. Consulting Eq. (4), it is seen that the two interactions−the dynamically screened Coulomb interaction induced by electrons and the LO phonon-induced interaction−play a part to the total retarded longitudinal susceptibility, represented by $\tilde{\chi}^{(t)}_{\boldsymbol{q}}(t_p;\omega) = \tilde{\chi}_{\boldsymbol{q}}(t_p;\omega) + \tilde{\chi}'_{\boldsymbol{q}}(t_p;\omega)$. Here, $\tilde{\chi}^{(t)}_{\boldsymbol{q}}(t_p;\omega)$, $\tilde{\chi}_{\boldsymbol{q}}(t_p;\omega)$, and $\tilde{\chi}'_{\boldsymbol{q}}(t_p;\omega)$ show the Fourier transforms of $\chi^{(t)}_{\boldsymbol{q}}(t_p+\tau,t_p)$, $\chi_{\boldsymbol{q}}(t_p+\tau,t_p)$, and $\chi'_{\boldsymbol{q}}(t_p+\tau,t_p)$ with respect to time $\tau$ into the frequency $\omega$-domain, respectively. $\tilde{\chi}_{\boldsymbol{q}}(t_p;\omega)$ is proportional to $|\boldsymbol{q}|^2$ in the small-$\boldsymbol{q}$ limit. On the other hand, $\tilde{\chi}'_{\boldsymbol{q}}(t_p;\omega)$ is proportional to $|\boldsymbol{q}|^2$ for the Frölich interaction of long range, and $|\boldsymbol{q}|^4$ for the deformation potential interaction of short range. This fact reflects on $\bar{I}_{\boldsymbol{q}}(t_p;\omega)$, as it

should be; in nonpolar crystals, lattice absorption disappears in the limit of a dipole transition accompanying momentum transfer $\boldsymbol{q} = 0$, since spatial inversion symmetry exists.

Figure 2 shows $\bar{I}_{\boldsymbol{q}}(t_p;\omega)$ of Si and GaAs at probe time $t_p$ = 15, 65, and 100 fs. The contribution from $\tilde{\chi}_{\boldsymbol{q}}(t_p;\omega)$ and $\tilde{\chi}'_{\boldsymbol{q}}(t_p;\omega)$ are separately represented by blue and green lines, respectively, and red lines represent the total one. The contribution of $\tilde{\chi}_{\boldsymbol{q}}(t_p;\omega)$ is mostly dominated by the $\alpha_1$ mode, whereas that of $\tilde{\chi}'_{\boldsymbol{q}}(t_p;\omega)$ is dominated by the $\alpha_2$ mode. $\tilde{\chi}_{\boldsymbol{q}}(t_p;\omega)$ is ascribed to electronic excitation through optical interband transitions. $\bar{I}_{\boldsymbol{q}}(t_p;\omega)$ includes structureless spectra due to the continuum modes $\{\beta\}$, which are almost constant in $\omega$ of concern. In both $\bar{I}_{\boldsymbol{q}}(t_p;\omega)$'s of Si and GaAs, the formation of spectral peaks is due only to $\tilde{\chi}'_{\boldsymbol{q}}(t_p;\omega)$. The width of the spectral peaks follows the relaxation time due to phonon anharmonicity, which is set to 0.27 meV in the calculation, rather than natural spectral width.

Figure 2(a) represents $\bar{I}_{\boldsymbol{q}}(t_p;\omega)$ of Si at $t_p = 15$ fs. The spectrum is dominated by the contribution from $\tilde{\chi}_{\boldsymbol{q}}(t_p;\omega)$ attributed to the $\alpha_1$ mode; $\tilde{\chi}^{(t)}_{\boldsymbol{q}}(t_p;\omega) \approx \tilde{\chi}_{\boldsymbol{q}}(t_p;\omega)$, and the spectrum shows monotonous reduction in $\omega$. On the other hand, the contribution from $\tilde{\chi}'_{\boldsymbol{q}}(t_p;\omega)$ is negligible since it is proportional to $|\boldsymbol{q}|^4$. In Fig. 2(b), the contribution from $\tilde{\chi}_{\boldsymbol{q}}(t_p;\omega)$ becomes small owing to the relaxation of the induced carrier density, attributed to $T_{\boldsymbol{k}\boldsymbol{q}bb'}$ in Eq. (2). Consequently, the contribution from $\tilde{\chi}_{\boldsymbol{q}}(t_p;\omega)$ is comparable with that from $\tilde{\chi}'_{\boldsymbol{q}}(t_p;\omega)$. It is remarked that asymmetric spectrum with a dip followed by a peak appears, which is characteristic of FR . This spectral profile contrasts with the symmetric line shape in Fig. 2(c) at $t_p = 100$ fs, where the spectrum is governed by $\tilde{\chi}'_{\boldsymbol{q}}(t_p;\omega)$; $\tilde{\chi}^{(t)}_{\boldsymbol{q}}(t_p;\omega) \approx \tilde{\chi}'_{\boldsymbol{q}}(t_p;\omega)$.

Regarding $\bar{I}_{\boldsymbol{q}}(t_p;\omega)$ of GaAs, Fig. 2(d) shows spectra at $t_p = 15$ fs with a discernible peak attributed to the $\alpha_2$ mode. The contributions from $\tilde{\chi}_{\boldsymbol{q}}(t_p;\omega)$ of the background continuum and $\tilde{\chi}'_{\boldsymbol{q}}(t_p;\omega)$ of the peak are comparable order because both are proportional to $|\boldsymbol{q}|^2$. Figure 2(e) shows the spectrum at $t_p = 65$ fs governed by $\tilde{\chi}'_{\boldsymbol{q}}(t_p;\omega)$, and a symmetric profile is obtained, which is different a lot from that of Si shown in Fig. 2(b). Figure 2(f) shows the spectrum at $t_p = 100$ fs representing the similar profile to that in Fig. 2(c).

It is possible to elucidate the origin of the occurrence of the asymmetric spectral profile shown in Fig. 2(b), that is, the transient FR by inspection of the details of the numerical calculation, namely, an analytic expression of the retarded longitudinal susceptibility, though not shown here. According to the procedures, major difference between the results of Si and GaAs originates just from the phase factor of the effective coupling constant $M_{\boldsymbol{q}\beta} = |M_{\boldsymbol{q}\beta}|e^{i\phi_{\boldsymbol{q}\beta}}$, apart from trivial difference of material parameters. $M_{\boldsymbol{q}\beta}$ is attributed to the LO phonon induced deformation potential interaction $g_{b\boldsymbol{q}} = g^D_{b\boldsymbol{q}}$ that is real in non-polar crystals, and the Fröhlich interaction $g_{b\boldsymbol{q}} = g^F_{b\boldsymbol{q}}$ that is pure imaginary in polar crystals. It is remarked that in GaAs, the contribution of the deformation potential interaction in $M_{\boldsymbol{q}\beta}$ is approximately an order of one thousand times smaller than that of the Fröhlich interaction in the present calculations. Actually, $\phi_{\boldsymbol{q}\beta}$ is determined by the phases of $g^D_{\boldsymbol{q}}$ and $g^F_{b\boldsymbol{q}}$; $\phi_{\boldsymbol{q}\beta} = 0, \pi$ for Si, whereas $\phi_{\boldsymbol{q}\beta} = \pm\pi/2$ for GaAs.

Now, we examine how the difference of $M_{\boldsymbol{q}\beta}$ influences the line shape of $\bar{I}_{\boldsymbol{q}}(t_p;\omega)$ with the PQ picture. The LO phonon discrete state $\alpha_2$ is embedded in the quasiboson continuum state $\beta$. They can be resonantly coupled, leading to the formation of the FR state of the PQ. As shown in Fig. 1(b), we have the two transition processes. One is a direct process through an optical transition matrix $D^{(c)}_{\boldsymbol{q}\beta}$ from the quasiboson state to the PQ ground state. The other is a two-step resonant process, that is, from $\beta$ to $\alpha_2$ mediated by $M^*_{\boldsymbol{q}\beta}$, and a deexcitation from $\alpha_2$ to the ground state follows it through an optical transition denoted by $D^{(r)}_{\boldsymbol{q}\alpha_2}$. Consulting Shore's model [18], $\bar{I}_{\boldsymbol{q}}(t_p;\omega)$ is provided in the vicinity of $\omega \approx \omega_{\boldsymbol{q}}$ as

$$\bar{I}_{\boldsymbol{q}}(t_p;\omega) \approx \mathcal{C}_{\boldsymbol{q}\beta} + \frac{\mathcal{A}_{\boldsymbol{q}\alpha_2}(\omega - \omega_{\boldsymbol{q}}) + \mathcal{B}_{\boldsymbol{q}\alpha_2}\Gamma_{\boldsymbol{q}\alpha_2}/2}{(\omega - \omega_{\boldsymbol{q}})^2 + (\Gamma_{\boldsymbol{q}\alpha_2}/2)^2}, \tag{6}$$

where the density of state of the quasiboson and the natural spectral width are provided by $\rho_{\boldsymbol{q}\alpha_2}$

and $\Gamma_{\boldsymbol{q}\alpha_2} = 2\pi\rho_{\boldsymbol{q}\alpha_2}|M_{\boldsymbol{q}\alpha_2}|^2$, respectively. Further, $M_{\boldsymbol{q}\alpha_2}$ is the coupling matrix at $\mathcal{E}_{\boldsymbol{q}\beta} = \omega_{\boldsymbol{q}}$. We obtain Shore's spectral parameters represented by $\mathcal{A}_{\boldsymbol{q}\alpha_2}$, $\mathcal{B}_{\boldsymbol{q}\alpha_2}$, and $\mathcal{C}_{\boldsymbol{q}\beta}$ as

$$\begin{cases} \mathcal{A}_{\boldsymbol{q}\alpha_2} = 2|D^{(c)}_{\boldsymbol{q}\beta}||D^{(r)}_{\boldsymbol{q}\alpha_2}||M_{\boldsymbol{q}\beta}|\cos\phi_{\boldsymbol{q}\beta} \\ \mathcal{B}_{\boldsymbol{q}\alpha_2} = -2|D^{(c)}_{\boldsymbol{q}\beta}||D^{(r)}_{\boldsymbol{q}\alpha_2}||M_{\boldsymbol{q}\beta}|\sin\phi_{\boldsymbol{q}\beta} + |D^{(r)}_{\boldsymbol{q}\alpha_2}|^2|M_{\boldsymbol{q}\beta}|^2/(\Gamma_{\boldsymbol{q}\alpha_2}/2) \\ \mathcal{C}_{\boldsymbol{q}\beta} = |D^{(c)}_{\boldsymbol{q}\beta}|^2 \end{cases} \tag{7}$$

The Fano's asymmetric $q$ parameter [11] is obtained by means of Shore's parameters as $q_{\boldsymbol{q}\alpha_2}(t_p) = r_{\boldsymbol{q}\alpha_2}(t_p) + \sigma_{\boldsymbol{q}\alpha_2}(t_p)\sqrt{[r_{\boldsymbol{q}\alpha_2}(t_p)]^2 + 1}$ with $r_{\boldsymbol{q}\alpha_2}(t_p) = \mathcal{B}_{\boldsymbol{q}\alpha_2}/\mathcal{A}_{\boldsymbol{q}\alpha_2}$ and $\sigma_{\boldsymbol{q}\alpha_2}(t_p) = \mathcal{A}_{\boldsymbol{q}\alpha_2}/|\mathcal{A}_{\boldsymbol{q}\alpha_2}|$, and $\mathcal{C}_{\boldsymbol{q}\beta}$ represents a continuum background.

The spectral profile depends on $\mathcal{A}_{\boldsymbol{q}\alpha_2}$. On the occasion of $\phi_{\boldsymbol{q}\beta} = \pm\pi/2$, $\mathcal{A}_{\boldsymbol{q}\alpha_2} = 0$ and the spectral profile of $\bar{I}_{\boldsymbol{q}}(t_p;\omega)$ becomes symmetric with $|q_{\boldsymbol{q}\alpha_2}(t_p)|$ infinite. This situation corresponds to the line shape of GaAs in Fig. 2(e). When $\phi_{\boldsymbol{q}\beta} \neq \pm\pi/2$, both $\mathcal{A}_{\boldsymbol{q}\alpha_2}$ and $\mathcal{B}_{\boldsymbol{q}\alpha_2}$ are finite, and an asymmetric spectral profile appears with $|q_{\boldsymbol{q}\alpha_2}(t_p)|$ finite. The line shape of Si in Fig. 2(b) with $\phi_{\boldsymbol{q}\beta} = 0$, $\pi$ is categorized into this case. For Figs. 2(c) and 2(f), because $D^{(c)}_{\boldsymbol{q}\beta}$ and $|M_{\boldsymbol{q}\beta}|$ are negligible, $\bar{I}_{\boldsymbol{q}}(t_p;\omega)$ is dominated by the second term of the expression of $\mathcal{B}_{\boldsymbol{q}\alpha_2}$. As a result, the spectral profile becomes symmetric. In conclusion, the effective coupling constant $M_{\boldsymbol{q}\beta}$ around $\mathcal{E}_{\boldsymbol{q}\beta} \approx \omega_{\boldsymbol{q}}$ plays a key part in the occurrence of the transient FR, and the spectral profile is strongly dependent on $\phi_{\boldsymbol{q}\beta}$ as far as $|M_{\boldsymbol{q}\beta}|$ is finite.

### 3.2 Irregular Oscillatory-Patterns in the Early-Time Region

Next, we show the calculated results of the oscillatory patterns $Q_{\boldsymbol{q}}(\tau)$ for undoped Si. The pulse envelop function $f(t)$ is set to a Gaussian-shape with $\tau_L = 10$ fs. Here, it should be noted that we investigated $\bar{I}_{\boldsymbol{q}}(t_p;\omega)$ shown in the previous section by solving the multichannel scattering problem. The scheme is based on the approximation that the effects of the interband density matrices $\bar{\rho}_{b\bar{b}\boldsymbol{k}}$ are partly neglected so as to solve the Hermitian problem substituted for the non-Hermitian problem of $h_{\boldsymbol{q}}$. This approximation scheme is justified for the case of the relatively weak excitation conditions. In the present scheme, we incorporate these neglected effects into calculations. However as the price to be paid, the more tractable eigenvalue problem takes the place of the scattering problem to be solved just for the sake of simplicity. We consider an integrated equation of motion of the phonon, the single-particle excitations in interbands, and the plasmon whose creation operator is defined by $\mathcal{B}^\dagger_{\boldsymbol{q}}$; $-id/dt[c^\dagger_{\boldsymbol{q}}, \bar{A}^\dagger_{\boldsymbol{q}}(\boldsymbol{k}b\bar{b})\cdots, \mathcal{B}^\dagger_{\boldsymbol{q}}] = [c^\dagger_{\boldsymbol{q}}, \bar{A}^\dagger_{\boldsymbol{q}}(\boldsymbol{k}b\bar{b})\cdots, \mathcal{B}^\dagger_{\boldsymbol{q}}]\bar{\mathcal{Z}}_{\boldsymbol{q}}$. $\bar{\mathcal{Z}}_{\boldsymbol{q}}$ represents a non-Hermitian matrix, though the explicit form is not shown here. From now on, the indices of $ph$, $pl$, and $(\boldsymbol{k}b\bar{b})$ represent the phonon, the plasmon, and the single-particle excitation in interbands, respectively. We solve the left and right eigenvalue problems of $\bar{\mathcal{Z}}_{\boldsymbol{q}}$ with time $t$ fixed as $\mathcal{V}^{L\dagger}_{\boldsymbol{q}j}\bar{\mathcal{Z}}_{\boldsymbol{q}} = E_{\boldsymbol{q}j}\mathcal{V}^{L\dagger}_{\boldsymbol{q}j}$ and $\bar{\mathcal{Z}}_{\boldsymbol{q}}\mathcal{V}^R_{\boldsymbol{q}j} = \mathcal{V}^R_{\boldsymbol{q}j}E_{\boldsymbol{q}j}$, where $\{j\} = (ph, \{\boldsymbol{k}b\bar{b}\}, pl)$. $E_{\boldsymbol{q}j}$ is the $j$th eigenvalue, and $\mathcal{V}^L_{\boldsymbol{q}j}$ and $\mathcal{V}^R_{\boldsymbol{q}j}$ are the associated biorthogonal eigenvectors. Thus, the PQ operator $P^\dagger_{\boldsymbol{q}j}$ is introduced as $P^\dagger_{\boldsymbol{q}j} = c^\dagger_{\boldsymbol{q}}\mathcal{V}^R_{\boldsymbol{q}ph\,j} + \mathcal{B}^\dagger_{\boldsymbol{q}}\mathcal{V}^R_{\boldsymbol{q}pl\,j} + \sum_{\boldsymbol{k}b}\bar{A}^\dagger_{\boldsymbol{q}}(\boldsymbol{k}b\bar{b})\mathcal{V}^R_{\boldsymbol{q}(\boldsymbol{k}b\bar{b})j}$.

In Figs. 3(a) and 3(b), we present the results of $\Theta_{\boldsymbol{q}}(\tau)$ and $C_{\boldsymbol{q}}(\tau)$ at $\tau = 20$ fs in the ETR as a function of $\Omega_{0cv}$, respectively, with $\Delta = 0$ and $-136$ meV. Both $\Theta_{\boldsymbol{q}}(\tau)$ and $C_{\boldsymbol{q}}(\tau)$ for $\Delta = 0$ meV represent irregular changes with cusp structures at $\Omega_{0cv} = \Omega^{(C1)}_{0cv} \equiv 82$ meV and $\Omega^{(C2)}_{0cv} \equiv 286$ meV. Further, the envelopes of both functions show steep changes around $\Omega_{0cv} = 350$ meV. In contrast, the behaviors of $\Theta_{\boldsymbol{q}}(\tau)$ and $C_{\boldsymbol{q}}(\tau)$ for $\Delta = -136$ meV are moderate over $\Omega_{0cv}$.

For the more precise interpretation of the results, we evaluate $\mathrm{Re}[E_{\boldsymbol{q}j}(\tau)]$ at $\tau = 20$ fs as a function of $\Omega_{0cv}$. Figure 3(c) shows the calculated results for $\Delta = 0$ meV, where the eigenvalues of $j = ph$ and $j = pl$ modes are represented by filled and open red squares, respectively. The plasma frequencies defined by $\omega_{\boldsymbol{q}pl}(\tau)$ for $\Delta = 0$ meV and $-136$ meV are also shown by red and blue dash lines, respectively. $\omega_{\boldsymbol{q}pl}(\tau)$ for $\Delta = 0$ meV obviously coincides with $\omega_{\boldsymbol{q}}$ at $\Omega_{0cv} = \Omega^{(C1)}_{0cv}$ and $\Omega^{(C2)}_{0cv}$, and it leads to anticrossings between $\mathrm{Re}[E_{\boldsymbol{q}ph}(\tau)]$ and $\mathrm{Re}[E_{\boldsymbol{q}pl}(\tau)]$.

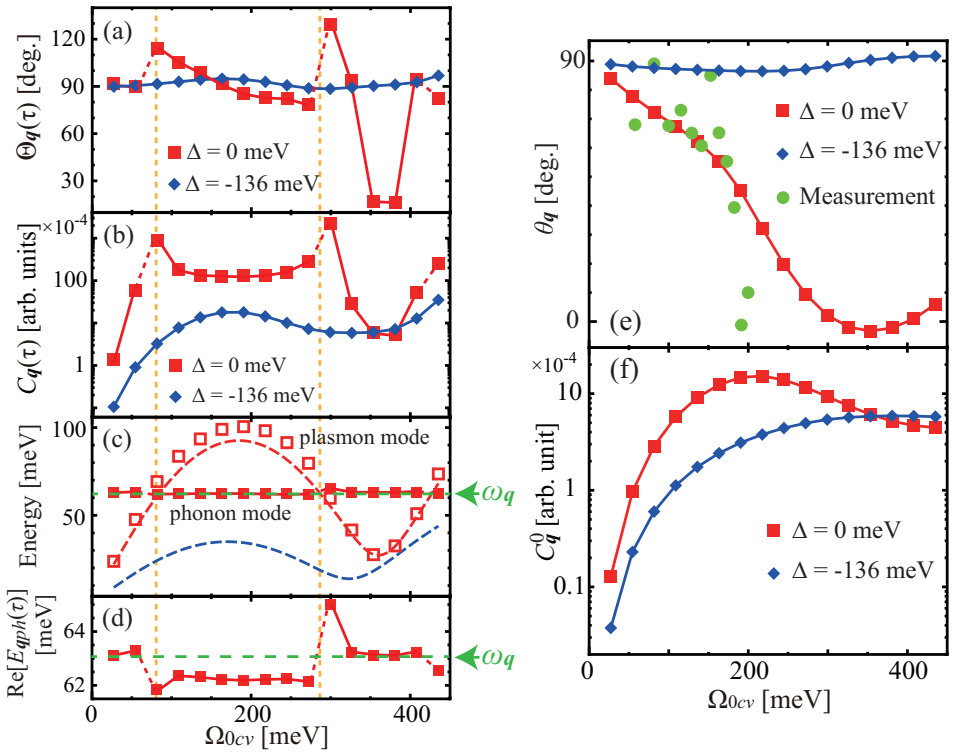


Figure 3: (a) $\Theta_{\boldsymbol{q}}(\tau)$, (b) $C_{\boldsymbol{q}}(\tau)$, and (c) The real parts of $E_{\boldsymbol{q}ph}(\tau)$ and $E_{\boldsymbol{q}pl}(\tau)$ as a function of $\Omega_{0cv}$ (in the unit of meV). (d) The enlarged view of Re$[E_{\boldsymbol{q}ph}(\tau)]$ around the phonon energy in panel (c). In panels (a)-(d), $\tau = 20$ fs and the detuning $\Delta = 0$ and $-136$ meV. (e) $\theta_{\boldsymbol{q}}$ and (f) $C^0_{\boldsymbol{q}}$ as a function of $\Omega_{0cv}$. Experimental data of $\theta_{\boldsymbol{q}}$ [3] are also shown by green circles. (From Ref. [15] with partial modification.)

Figure 3(d) shows the enlarged view of Re$[E_{\boldsymbol{q}ph}(\tau)]$ in Fig. 3(c). The difference between Re$[E_{\boldsymbol{q}ph}(\tau)]$ and $\omega_{\boldsymbol{q}}$ shows the self-energy, which is attributed almost to the interaction between the phonon and the plasmon; the effects of the single-particle excitations would be much smaller. The self-energy for $\Delta = 0$ meV alters steeply at $\Omega_{0cv} = \Omega^{(C1)}_{0cv}$ and $\Omega^{(C2)}_{0cv}$, and these positions are in agreement with those of the manifestation of the cusp structures in Figs. 3(a) and 3(b). Therefore it is concluded that the anomalies in $\Theta_{\boldsymbol{q}}(\tau)$ and $C_{\boldsymbol{q}}(\tau)$ are clearly ascribed to the anticrossings resulting from the energetically *resonant* interaction between the phonon and the plasmon of the photoexcited carriers. Regarding the case for $\Delta = -136$ meV, such anomalies are not obtained since $\omega_{\boldsymbol{q}} > \omega_{\boldsymbol{q}pl}(\tau)$ within the present range of $\Omega_{0cv}$.

Moreover in Fig. 3(c), $\omega_{\boldsymbol{q}pl}(\tau)$ denoted by a dash line oscillates with a period of approximately 350 meV. This results from the interband Rabi flopping of the photoexcited carriers, where it ends at $\tau \approx \tau_L/2$, because in the present calculations for $\tau_L = 10$ fs, $\Omega_{0cv}$ of $2\pi$-pulse is approximately provided by $\Omega_{0cv} = \Omega^{(2\pi)}_{0cv} \equiv 388$ meV and that of $\pi$-pulse is provided by $\Omega^{(\pi)}_{0cv} = \Omega^{(2\pi)}_{0cv}/2$ except for the Coulomb correction. Therefore, the evident alterations of $\Theta_{\boldsymbol{q}}(\tau)$ and $C_{\boldsymbol{q}}(\tau)$ around $\Omega_{0cv} = \Omega^{(2\pi)}_{0cv}$ for $\Delta = 0$ meV shown in Figs. 3(a) and 3(b) result from the Rabi oscillation.

We show the results of the initial phase $\theta_{\boldsymbol{q}}$ and the asymptotic amplitude $C^0_{\boldsymbol{q}}$ as a function of $\Omega_{0cv}$ in Figs. 3(e) and 3(f), respectively. It is seen that the Rabi-oscillatory patterns still appear in both of $\theta_{\boldsymbol{q}}$ and $C^0_{\boldsymbol{q}}$ for $\Delta = 0$ meV around $\Omega_{0cv} = \Omega^{(2\pi)}_{0cv}$, whereas the cusp structures vanish because the plasmon-phonon coupling is suppressed due to the carrier relaxation. The experimental results of $\theta_{\boldsymbol{q}}$, which represent the dependence on the pump fluence for lightly $n$-

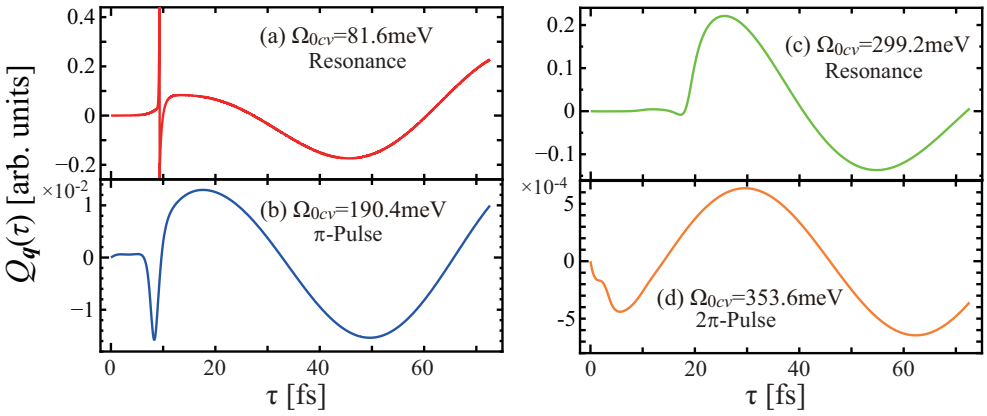


Figure 4: $Q_{\boldsymbol{q}}(\tau)$ as a function of $\tau$ (in the unit of fs) in the ETR at four specific $\Omega_{0cv}$'s provided in panels (a)-(d). (From Ref. [15] with partial modification.)

doped Si [3], are also shown in Fig. 3(e). As the fluence increases, $\theta_{\boldsymbol{q}}$ varies from 90° to the vicinity of 0°. The result is consistent with the calculated one for $\Delta = 0$ meV.

Figures 4(a)-4(d) represent the calculated results of $Q_{\boldsymbol{q}}(\tau)$ in the ETR as a function of $\tau$ for $\Delta = 0$ meV. Here $\Omega_{0cv}$ is set to $\Omega_{0cv}^{(C1)\prime} \equiv 81.6$ meV, $\Omega_{0cv}^{(\pi)\prime} \equiv 190.4$ meV, $\Omega_{0cv}^{(C2)\prime} \equiv 299.2$ meV, and $\Omega_{0cv}^{(2\pi)\prime} \equiv 353.6$ meV, in the proximity to $\Omega_{0cv}^{(C1)}$, $\Omega_{0cv}^{(\pi)}$, $\Omega_{0cv}^{(C2)}$, and $\Omega_{0cv}^{(2\pi)}$, respectively. As shown in Fig. 3(c), the number of excited carriers is maximized at $\Omega_{0cv} = \Omega_{0cv}^{(\pi)\prime}$, and minimized at $\Omega_{0cv} = \Omega_{0cv}^{(2\pi)\prime}$ of the four. At $\Omega_{0cv} = \Omega_{0cv}^{(C1)\prime}$ and $\Omega_{0cv}^{(C2)\prime}$, owing to the plasmon-phonon resonant coupling, $Q_{\boldsymbol{q}}(\tau)$'s show irregular oscillatory patterns from a simple sinusoidal function with a period of $2\pi/\omega_{\boldsymbol{q}} = 66$ fs. The transitory amplitudes $C_{\boldsymbol{q}}(\tau)$ at $\Omega_{0cv} = \Omega_{0cv}^{(C1)\prime}$ and $\Omega_{0cv}^{(C2)\prime}$ of the resonant conditions are approximately ten times larger than that at $\Omega_{0cv} = \Omega_{0cv}^{(\pi)\prime}$ of the $\pi$-pulse laser condition, whereas the asymptotic amplitudes $C_{\boldsymbol{q}}^0$ of the resonant conditions are several times smaller than that of $\pi$-pulse laser condition [see Fig. 3(b)]. Moreover, it is seen that the renormalized phase $\Theta_{\boldsymbol{q}}(\tau)$ changes anomalously, in particular at $\Omega_{0cv} = \Omega_{0cv}^{(C1)\prime}$; the phase varies rapidly over $2\pi$ around $\tau = 10$ fs, attributed presumably to the appearance of the resonant interaction. Besides, $Q_{\boldsymbol{q}}(\tau)$ of $\Omega_{0cv} = \Omega_{0cv}^{(\pi)\prime}$ deviates from a simple harmonics due to the maximized carrier inversion. In contrast, $\Theta_{\boldsymbol{q}}(\tau)$ and $C_{\boldsymbol{q}}(\tau)$ of $\Omega_{0cv} = \Omega_{0cv}^{(2\pi)\prime}$ are almost unchanged, and gradually approaches the asymptotes; $Q_{\boldsymbol{q}}(\tau)$ represents a damped harmonic oscillation in most of the time-region.

## 4 Conclusions

A fully quantum mechanical model based on the PQ picture for the CP generation in semiconductors is constructed. In this model, the LO phonon, the plasmon of the collective excitation, and the electron-hole continua of the single-particle excitation are taken into consideration. Thereby, quantum mechanical effects inherent in the interactions among these modes are theoretically revealed, that is, the optically nonlinear and transient FR, the anomalous oscillatory pattern ascribed to the plasmon-phonon resonant interaction, and the Rabi flopping. It is found that these quantum effects enrich the underlying physics of the CP generation in the ETR.

The transient FR is manifested in the transient induced photoemission spectra; an asymmetric spectral profile appears in Si, whereas not in GaAs. The distinct profiles of Si and GaAs are ascribed to the effective quasiboson-phonon coupling $M_{\boldsymbol{q}\beta}$; by consulting Shore's model, the spectral profiles are strongly dependent on $\arg M_{\boldsymbol{q}\beta}$, and the asymmetry in spectra is due to the

deformation potential interaction, and the Fröhlich interaction leads to the symmetric profile. After the ETR of $|M_{\boldsymbol{q}\beta}| \approx 0$, the profiles become symmetric in both of Si and GaAs.

The effects of the resonant coupling between the plasmon and the phonon, and the Rabi flopping also appear in the ETR. In the CP displacement function of Si, irregular oscillatory patterns due to the plasmon-phonon resonance are observed just in the ETR. This resonance effect is expected to be verified experimentally by reducing the masking effect ascribed to coherent artifacts. Further, the resonance effect would be enhanced in polar crystals such as GaAs because the Fröhlich interaction is much larger than the deformation potential interaction. On the other hand, the Rabi flopping is also manifested after the ETR, and discernible in experiments through the measure of the initial phase and the asymptotic amplitude as a function of the Rabi frequency up to more than the one of the $2\pi$-pulse laser.

## References


[1] A. V. Kuznetsov and C. J. Stanton, in *Ultrafast Phenomena in Semiconductors*, edited by K. T. Tsen (Springer-Verlag, Berlin, 2001) Chap. 7.

[2] M. Hase, M. Kitajima, A. M. Constantinescu, and H. Petek, Nature (London) **426**, 51 (2003).

[3] M. Hase, M. Katsuragawa, A. M. Constantinescu, and H. Petek, Nature Photon. **6**, 243 (2012).

[4] K. Ishioka, M. Kitajima, and O. V. Misochko, J. Appl. Phys. **100**, 093501 (2006).

[5] O. V. Misochko, K. Kisoda, K. Sakai, and S. Nakashima, Phys. Rev. B **61**, 4305 (2000).

[6] Y. -X. Yan, E. B. Gamble, and K. A. Nelson, J. Chem. Phys. **83**, 5391 (1985).

[7] H. J. Zeiger, J. Vidal, T. K. Cheng, E. P. Ippen, G. Dresselhaus, and M. S. Dresselhaus, Phys. Rev. B **45**, 768 (1992).

[8] D. M. Riffe and A. J. Sabbah, Phys. Rev. B **76**, 085207 (2007).

[9] G. A. Garrett, T. F. Albrecht, J. F. Whitaker, and R. Merlin, Phys. Rev. Lett. **77**, 3661 (1996).

[10] M. V. Lebedev, O. V. Misochko, T. Dekorsy, and N. Georgiev, J. Exp. Theor. Phys., **100**, 272 (2005).

[11] U. Fano, Phys. Rev. **124**, 1866 (1961).

[12] P. Gaal, W. Kuehn, K. Reimann, M. Woerner, T. Elsaesser, and R. Hey, Nature **450**, 1210 (2007).

[13] F. Cerdeira, T. A. Fjeldly, and M. Cardona, Phys. Rev. B **8**, 4734 (1973).

[14] Y. Watanabe, K. Hino, M. Hase and N. Maeshima, Phys. Rev. B **95**, 014301 (2017).

[15] Y. Watanabe, K. Hino, M. Hase and N. Maeshima, Phys. Rev. B **96**, 125204 (2017).

[16] W. Schäfer and M. Wegener, *Semiconductor Optics and Transport Phenomena* (Springer-Verleg, Berlin, 2002) Chaps. 2, 10 and 11.

[17] G. D. Mahan, *Many-Particle Physics* (Plenum, New York, 1981), Chaps. 4 and 5.

[18] B. W. Shore, Rev. Mod. Phys. **39**, 439 (1967).